CHEMISTRY
A EUROPEAN JOURNAL

DOI: 10.1002/chem.200700127

Circular Dichroism and Conformational Dynamics of Cephams and Their Carba and Oxa Analogues

Jadwiga Frelek,*[a] Patrycja Kowalska,[a] Marek Masnyk,[a] Arkadiusz Kazimierski,[a] Anna Korda,[a] Magdalena Woźnica,[a] Marek Chmielewski,[a] and Filipp Furche*[b]

Abstract: The biological activity of bicyclic β-lactam antibiotics depends strongly on the absolute configuration of the bridgehead carbon atom. Frelek and co-workers proposed an empirical helicity rule relating the configuration of the bridgehead carbon atom to the sign of the 220 nm band in the electronic circular dichroism (CD) spectrum of β-lactams. Here we use synthetic organic chemistry, CD spectroscopy, and time-dependent density functional theory (TDDFT) to investigate the validity of this structure–property relationship for eight model compounds. For conformationally flexible β-lactams, substantial thermal effects are found which must be included in calculations. To this end, we combine TDDFT calculations of CD with full quantum-mechanical Born–Oppenheimer molecular dynamics (MD) simulations for the first time. The CD spectra are sampled with ground-state density functional trajectories of up to 60 ps. The MD simulations show a surprisingly high sensitivity of the CD to the molecular conformation. On the other hand, the relation between CD and thermally averaged structural parameters is much less complex. While the helicity rule does not seem to hold for individual conformers, it is confirmed by the calculations for seven out of eight systems studied if thermally averaged CD spectra and structures are considered. Since thermal effects on CD can be larger than typical inherent inaccuracies of TDDFT, our results emphasize the need for a systematic treatment of conformational dynamics in CD calculations even for moderately flexible systems. Temperature-dependent CD measurements are very useful for this purpose. Our results also suggest that CD spectroscopy may be used as a sensitive probe of conformational dynamics if combined with electronic structure calculations.

Keywords: circular dichroism · density functional calculations · lactams · molecular dynamics · structure–activity relationships

Introduction

Since the introduction of penicillin onto the market in 1940, β-lactam antibiotics have remained the main pharmaceutical tool against bacterial infections.[1] The extensive use of penicillins and cephalosporins, however, has resulted in a rapid increase of bacterial resistance.[2] This has prompted the search for new structural variants of β-lactam antibiotics with enhanced activity and/or novel biological profile. Among the large number of antibiotics that have been synthesized and isolated, only compounds with *R* configuration of the bridgehead carbon atom have been found to display antibacterial activity.[3] The isolation of the potent β-lactamase inhibitor clavulanic acid (**i**) by Beecham[4] in 1976 and the synthesis of the oxacephems oxacephalotin (**ii**)[5] and oxacephamandol (**iii**)[6] (Scheme 1) by the Merck group, which are more active than the natural congeners, demonstrated that the high biological activity of β-lactam antibiotics does not depend on the presence of the sulfur atom in the molecule. Discovery of the clavams (4-oxapenams, **iv**) with *S* configuration of the bridgehead carbon atom (Scheme 1), which are active against a number of species of fungi,[7] showed that both enantiomeric families of β-lactam antibiotics may display interesting therapeutic properties. Thus, reliable knowledge of the absolute stereostructure of such bioactive compounds is crucial for further improvement of the bioac-

[a] Prof. Dr. J. Frelek, P. Kowalska, Dr. M. Masnyk, Dr. A. Kazimierski, Dr. A. Korda, M. Woźnica, Prof. Dr. M. Chmielewski
Institute of Organic Chemistry of the Polish Academy of Sciences
Kasprzaka 44, 01-224 Warsaw (Poland)
Fax: (+48) 22-632-6681
E-mail: frelek@icho.edu.pl

[b] Dr. F. Furche
Institut für Physikalische Chemie
Universität Karlsruhe (TH)
Kaiserstraße 12, 76128 Karlsruhe (Germany)
Fax: (+49) 721-608-7225
E-mail: filipp.furche@chem-bio.uka.de

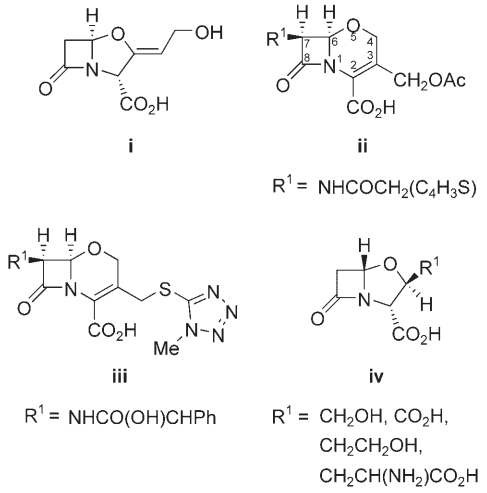

Scheme 1. Some representative oxa analogues of penicillins and cephalosphorins.

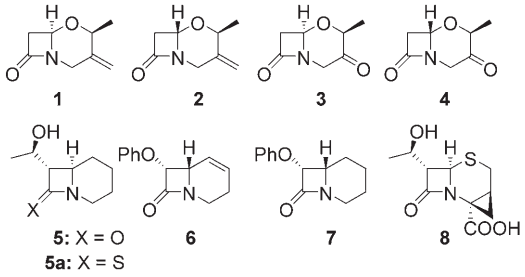

Scheme 2. Investigated model cepham analogues **1**–**8**.

tivity by directed synthetic modifications. Moreover, β-lactams are useful synthetic intermediates for a number of other biologically active heterocycles such as indolizidines, pyrrolizidines, pyrrolidines, pyrroles, taxoids, and macrolides.[8] A practical method that would allow unequivocal, fast, and reliable determination of the absolute configuration of β-lactams and closely related compounds is therefore highly desirable.

Circular dichroism spectroscopy is a convenient and sensitive technique to probe the stereochemistry of azetidinones and their polycyclic derivatives.[9] To assign the absolute configuration by CD spectroscopy, a theoretical model is needed that correlates the observed spectrum to a three-dimensional molecular structure. Recently, Frelek and coworkers reported a correlation between the stereostructure of 5-dethia-5-oxacephams and their circular dichroism.[10] As a result, a simple helicity rule was proposed which assigns the absolute configuration at the ring junction carbon atom C(6) based on the sign of the CD band at around 220 nm. According to this rule, a positive sign of the 220 nm Cotton effect (CE) corresponds to an *R* absolute configuration at the bridgehead carbon atom, whereas a negative sign of the same CE is related to a 6*S* absolute configuration. The rule was experimentally demonstrated to be correct for a variety of oxacephams.[10,11] Moreover, it was shown to hold for clavams as oxa analogues of penicillins.[12] However, the helicity rule was established empirically on the basis of X-ray structures and the tentative assignment of the electronic transition at approximately 220 nm to an $n\rightarrow\pi^*$ amide transition in the azetidinone system.[10,12] Despite its appealing simplicity and its apparent success, the underlying assumptions of conformational rigidity and electronic decoupling of the amide chromophore require further validation.

In the present work, we employ time-dependent density functional calculations to investigate the relation between molecular structure and CD for the set of eight β-lactam model compounds shown in Scheme 2. These model compounds cover the therapeutically important classes of oxacephams (**1**–**4**) and carbacephams (**5**–**7**); cepham derivative **8** was included for comparison. For a given molecular conformation, TDDFT provides a detailed picture of the electronic structure, which in turn is the key to a quantitative treatment of chiroptical properties. Thus, by comparing the computed CD spectra to the measured ones, we can infer conclusions on the stereochemistry of the β-lactams studied here. In particular, we can assign the absolute configuration of the crucial bridgehead carbon atom for seven out of eight compounds, which provides an independent test of the helicity rule.

A second important motivation of the present paper concerns the treatment of thermal effects in simulated CD spectra. These effects are small for rigid molecules, because the CD spectrum at finite temperature is dominated by the CD spectrum of the energetically lowest conformer. While TDDFT calculations are now routinely used to assign the CD spectra of rigid molecules,[13] little was known about the performance of TDDFT for larger and flexible systems so far. For alanine and proline, a strong dependence on the molecular conformation has been observed in TDDFT gas-phase calculations of the optical rotation, which is closely related to CD.[14] Many chiral molecules of natural and synthetic origin are nonrigid; therefore, it is of considerable interest whether thermal effects on the CD spectrum of such systems can be quantified and systematically included in TDDFT calculations. In the present work, we address this question by combining TDDFT calculations with direct Born–Oppenheimer finite-temperature molecular dynamics (MD) simulations using ground-state DFT. This involves sampling CD spectra over tens of thousands of time steps, and builds on previously developed efficient ground-state[15,16] and TDDFT[17] implementations. While classical force-field trajectories have been used to sample CD spectra of flexible molecules in the past,[18] the present work is, to the best of our knowledge, the first attempt to simulate CD spectra of biologically relevant molecules based on a fully quantum mechanical potential-energy surface from density functional theory. A similar route has been pursued by Bernasconi et al.,[19] who sampled the TDDFT absorption spectra of Cu^+ and Ag^+ in solution using Car–Parrinello MD.[20] In the present work, solvent effects are approximately included by the COSMO continuum solvation model.[21] As we will show, some cepham derivatives are less rigid than

expected, and finite temperature can change their CD spectra dramatically. Our simulations account for vibronic effects in a classical approximation; the importance of these effects for CD[22] and for optical rotations[23] has recently been stressed.

Results and Discussion

General aspects: The CD data of cepham analogues **1**–**8** are collected in Table 1. Oxacephams **1** and **3** show a positive Cotton effect (CE) at around 220 nm, whilst oxacephams **2** and **4** have a negative CE in the same spectral region. According to the helicity rule, we expect a 6*R* configuration for **1** and **3**, and a 6*S* configuration for **2** and **4**.[10,12] This has been confirmed by X-ray structure analysis of oxacephams **2** and **3**.[24] The presence of the *exo*-methylene group at C(3) in **1** and **2** does not constitute any extension of the β-lactam chromophoric system. Therefore, the shape of the CD spectra of **1** and **2** around 220 nm does not differ in comparison to the saturated oxacephams described before.[10,12] However, the *exo*-methylene group contributes to the overall CD spectrum in the high-energy part of the spectrum, as discussed below. The presence of an additional Cotton effect at around 313 nm in oxacephams **3** and **4** is due to the carbonyl group at C(3). Despite the opposite configuration of the bridgehead carbon atom, this band has the same sign in both compounds.

Table 1. CD data of cepham analogues **1**–**8** in acetonitrile. ε is the molar decadic absorption coefficient, and λ_{max} the wavelength of the band maximum.

Compound	$\Delta\varepsilon$ [L mol^{-1} cm^{-1}] (λ_{max} [nm])		
1	−5.25 (196.0)	+11.41 (219.0)	
2	+2.82 (200.0)	−10.43 (219.0)	
3	−3.17 (197.5)	+7.22 (220.5)	−1.87 (314.0)
4	+1.14 (202.0)	−4.07 (224.0)	−1.55 (312.5)
5	−12.25 (194.0)	+11.19 (218.5)	
6	+9.77 (205.5)	−15.52 (223.0)	−0.94 (268.0)
7	+8.92 (200.5)	−8.48 (222.5)	−0.91 (268.5)
8	−9.56 (198.5)	+9.40 (223.0)	

Compounds **8** and **5** representing cepham and its carba analogue, respectively, behave similarly to oxacephams discussed before. In their CD spectra a positive CE at around 220 nm indicates a 6*R* configuration, in agreement with the helicity rule. In contrast, **6** and **7** with an *S* configuration at the bridgehead carbon atom have a negative 220 nm CD band, as suggested by the rule. Thus, it can be stated that compounds **5**–**8** fulfil the requirements of the helicity rule. Therefore, we can expect that the β-lactam unit in these compounds is nonplanar and that the sense of chirality of the chromophore is controlled by the 6*R* or 6*S* absolute configuration and is also the sign-determining factor for the 220 nm CD band. The X-ray data for cepham **8** indicate the skewness of the β-lactam unit by negative O(9)-C(8)-N(1)-C(2) and O(9)-C(8)-N(1)-C(6) torsion angles of −22.9 and −177.0°, respectively.[25] Therefore, a positive sign of the long-wavelength CD band is observed in its CD spectrum, in agreement with the helicity rule. The computed torsion angles $\measuredangle$(9,8,1,6) for compounds **1**–**8** provide corroborating evidence for the nonplanarity of the amide chromophore (Table 2). Additionally, we report $\measuredangle$(8,6,2,1) dihedral angles to quantify the pyramidalization of the amide nitrogen atom.

Table 2. Computed PBE0/SV(P) torsion and dihedral angles $\measuredangle$(9,8,1,6) and $\measuredangle$(8,6,2,1) in degrees. Values in parentheses denote thermal averages at 350 K.

Compound	$\measuredangle$(9,8,1,6)	$\measuredangle$(8,6,2,1)
1	−174	+19
2	+174	−20
3	−173	+20
4	(+175)	(−20)
5	(−177)	(+10)
6	(+172)	(−21)
7	(+173)	(−14)
8	−176	+14

Oxacephams 1 and 2: The computed lowest energy conformer of oxacepham **1** is shown in Figure 1. The six-membered ring is in a chair conformation, with the four-membered azetidin-2-one ring in equatorial position at C(6). Conformers with the azetidin-2-one ring in axial position at C(6) are substantially higher in energy and have no significance for the chiroptical properties of all compounds investigated here. This is in line with simple arguments based on steric strain. The methyl group at C(4) is in equatorial position, which is energetically favorable.

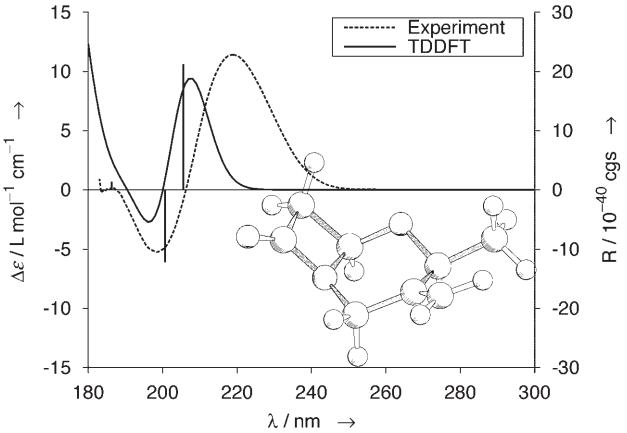

Figure 1. Computed structure of **1** and its simulated CD spectrum (denoted TDDFT) compared to experiment. ε is the molar decadic absorption coefficient, λ the wavelength, and *R* the computed rotatory strength. The spectrum was recorded in acetonitrile solution at room temperature.

The agreement between the simulated and experimental CD spectra is very satisfactory, and confirms the absolute configuration and the conformation of **1**. The band at 220 nm has mainly the character of an amide n(O)→π* tran-

sition. Its positive sign is predicted by both the helicity rule and the TDDFT calculations. The calculated band is slightly blue-shifted, which is not untypical of the PBE0 functional we use here; also, thermal effects may contribute to this discrepancy (see below). The weaker negative band at about 200 nm originates predominantly from a short-range charge-transfer transition out of the nitrogen lone pair into the methylene C–C π* orbital, with some C=C π→π* admixture. The intense positive C=C π→π* and amide n(N)→π* transitions are located at the blue end of the spectrum.

The notion of an "amide n(N)→π*" transition requires some clarification. In an unstrained planar amide, the nitrogen atom has a planar "sp^2" configuration and its lone pair is part of the delocalized π system. However, in the cephams and oxacephams investigated here, the nitrogen atom is partly pyramidalized due to steric constraints; compare the computed pyramidalization angles in Table 2. As the pyramidalization angle increases, the nitrogen lone pair decouples from the C=O π system and becomes localized at the nitrogen atom. Since the transition from an amide π orbital to a nitrogen lone pair is gradual, the "amide n(N)→π*" transition can be imagined as gradually evolving from the π→π* transition of planar amide chromophores as the nitrogen becomes nonplanar.

The lowest energy conformer of oxacepham **2** again exhibits a chair conformation of the six-membered ring. The inverted configuration of C(6) implies that the methyl substituent at C(4) now occupies an axial position. This intriguing result is supported by previous X-ray studies on **2**.[24] The TDDFT calculations predict a negative sign of the amide n(O)→π* transition at 220 nm (see Figure 2), which confirms the helicity rule in this case. The sign of the bands at 200 and 180 nm is inverted, too. Since **1** and **2** are diastereomers, this is not a trivial result.

It is instructive to ask whether internal rotation of **2** is possible such that the methyl group occupies an equatorial position. The resulting optimized structure is shown in Figure 3. This conformer is generated from the lowest energy structure in Figure 2 by a torsion that transforms the six-membered ring from the chair to a boat conformation. This boat conformer is computed to be about 2 kcal mol^{-1} higher in energy than the chair conformer. The boat conformer of **2** should therefore not have a significant thermal population at room temperature. This is supported by the computed CD spectrum (Figure 3), which shows sign inversion of the band at 220 nm relative to the chair conformer, in disagreement with the experimental CD spectrum.

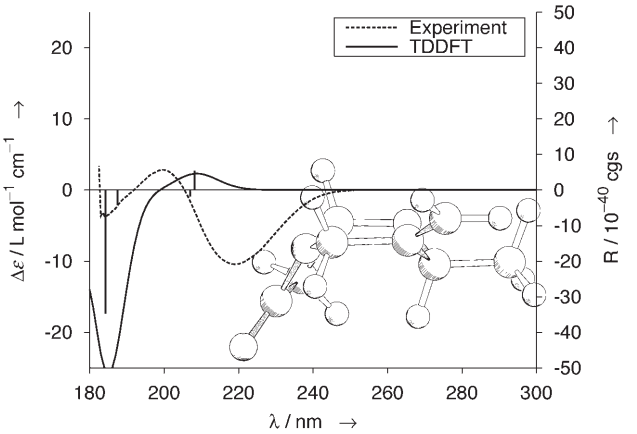

Figure 3. Computed structure of the boat conformer of **2** and its simulated CD spectrum compared to experiment. Details as in Figure 1.

The structure of the azetidin-2-one ring hardly changes going from the chair to the boat conformer of **2**. The torsion angle ∢(9,8,1,6) of the boat conformer is 175.6°, which is similar to that of 173.8° for the chair conformer. Other dihedral and torsion angles of the four-membered ring, for example, ∢(8,6,2,1) and ∢(9,8,1,2), agree within about 2°, too. According to the helicity rule, one would expect the same sign of the CD band at 220 nm for both conformers. The calculations suggest, however, that the helicity rule does not hold for the boat conformer.

Oxacephams 3 and 4: Figure 4 shows the optimized lowest energy structure found for oxacepham **3**. As expected from

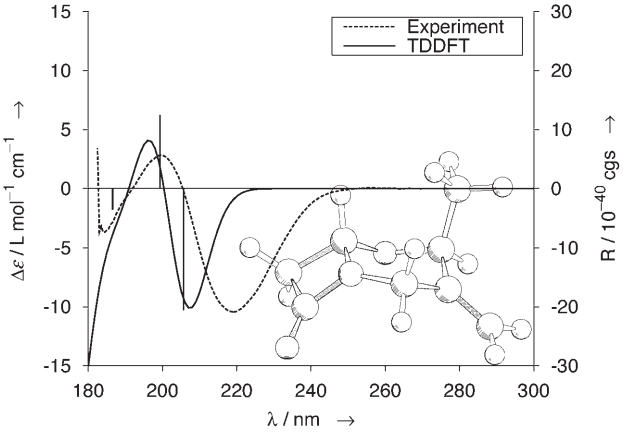

Figure 2. Computed structure of **2** and its simulated CD spectrum compared to experiment. Details as in Figure 1.

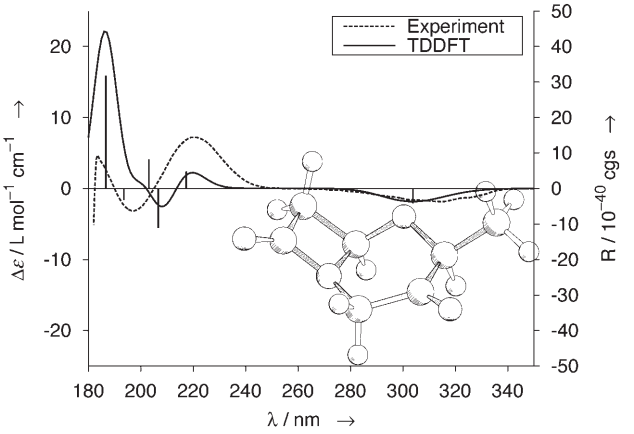

Figure 4. Computed structure of **3** and its simulated CD spectrum compared to experiment. Details as in Figure 1.

comparison with **1**, the six-membered ring has a chair conformation, and the methyl substituent at C(6) is in an equatorial position. This is fully consistent with the X-ray structure.[24] The experimental CD spectrum of **3** exhibits a weak negative band at about 320 nm, which is well reproduced by the calculations and can be assigned to an n→π* transition of the C(3)=O group. Strong mixing of the amide n(O)→π* transition with charge-transfer transitions between the amide and the C(3)=O chromophore leads to several transitions of low intensity which partly cancel. This is a difficult situation from the theoretical point of view, because small errors in the method or the basis set used can lead to dramatic changes in the computed intensity pattern. The sign of the band at 220 nm is therefore assigned somewhat tentatively by the calculations. Nevertheless, the more intense band at the blue end of the spectrum is clearly correct.

What about the boat conformation of the six-membered ring? The corresponding structure is a minimum (Figure 5),

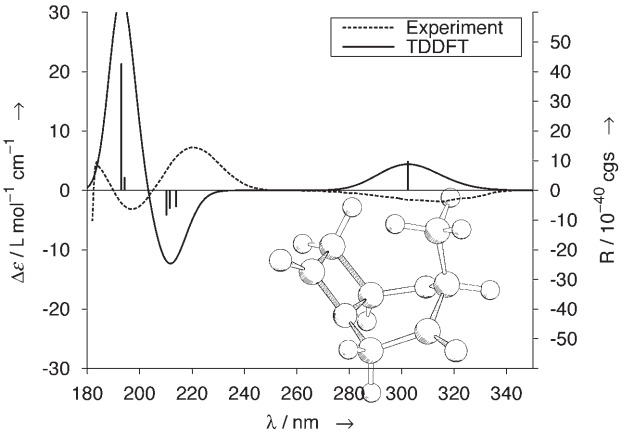

Figure 5. Computed structure of the boat conformer of **3** and its simulated CD spectrum compared to experiment. Details as in Figure 1.

but its energy is computed to be 3.3 kcal mol^{-1} higher than that of the chair conformer. This destabilization may be rationalized by the combined effect of the axial methyl substituent at C(4) and the boat conformation of the six-membered ring, both of which are energetically unfavorable. Although the structure of the azetidin-2-one moiety is almost unchanged in the boat conformer, the calculations predict an inversed sign of the CD band at 220 nm. Thus, the helicity rule apparently does not hold for the boat conformers. The conformational change also leads to sign inversion of the 320 nm carbonyl band. The computed CD spectrum of the boat conformer is in disagreement with experiment, consistent with its considerably higher energy.

Figure 6 shows the boat and chair conformers of **4**. The boat conformer is computed to be more stable by only 0.6 kcal mol^{-1} at the PBE0/SV(P) level; increasing the basis set to def2-TZVP yields 0.3 kcal mol^{-1}, an insignificant change. Thus, the boat and chair conformers of **4** are isoenergetic (within the accuracy of the computational method used here). The stabilization of the boat conformer in **4** may

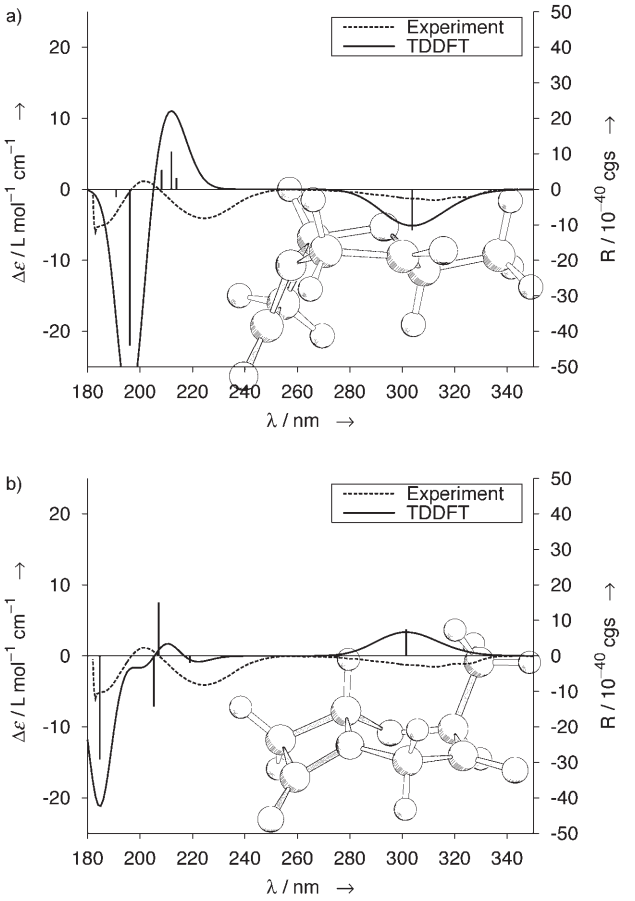

Figure 6. Computed structures of the boat (a) and chair (b) conformers of **4** and their simulated CD spectra compared to experiment. Details as in Figure 1.

be a consequence of the smaller size of the C(3)=O group compared to the C(3)=CH_2 group of **2**, reducing the energetically unfavorable interaction with the eclipsed methyl group at C(4) in the boat conformer.

As shown in Figure 6, the computed CD spectrum of either conformer of **4** does not match the experimental spectrum. For the boat conformer, the C(3)=O band at 320 nm is correct in sign, but the amide band at 220 nm has the incorrect sign. For the chair conformer, the computed amide band at 220 nm is correct (albeit somewhat weak), but the sign of the carbonyl band is wrong. This disagreement and the fact that both conformers are very close in energy suggest fast internal conversion of the two forms at room temperature. The corresponding torsion modes of the six-membered ring exhibit harmonic vibrational frequencies below 100 cm^{-1}, as was verified by force constant calculations. To check the hypothesis of fast conversion and to conclusively assign the experimental CD spectrum, we performed extensive MD simulations at a fixed temperature of 350 K. The simulation temperature was chosen to be slightly above room temperature to reduce the simulation time; further details are given in the Computational and Experimental Section.

Figure 7a shows the computed distribution of the 10,4,3,11 torsion angle. The carbon atom of the methyl group at C(4) is numbered 10, and the carbonyl oxygen atom bound to C(3) is numbered 11; $\measuredangle(10,4,3,11)$ is a good measure of the boat or chair character of **4**. For the boat conformer, its value is −16°, while it is −72° for the chair conformer. The broad distribution in Figure 7a indicates that the six-membered ring is mostly between boat and chair at 350 K. Indeed, the trajectories show that the barriers separating the two conformers are easily overcome at this temperature. To analyze the correlation between $\measuredangle(10,4,3,11)$ and the CD spectrum, we have computed conditional probability distributions of the CD band at 320 nm for various values of $\measuredangle(10,4,3,11)$ from our MD data (Figure 7b). In other words, the curves in Figure 7b approximately give the probability of observing a certain $\Delta\varepsilon$ value of the 320 nm band at fixed $\measuredangle(10,4,3,11)$. A more negative value of the torsion angle corresponding to greater chair character correlates with more positive values of the 320 nm band. Nevertheless, the distribution of the CD intensities is still rather broad. This indicates that structural parameters other than $\measuredangle(10,4,3,11)$ have considerable influence on the CD band at 320 nm.

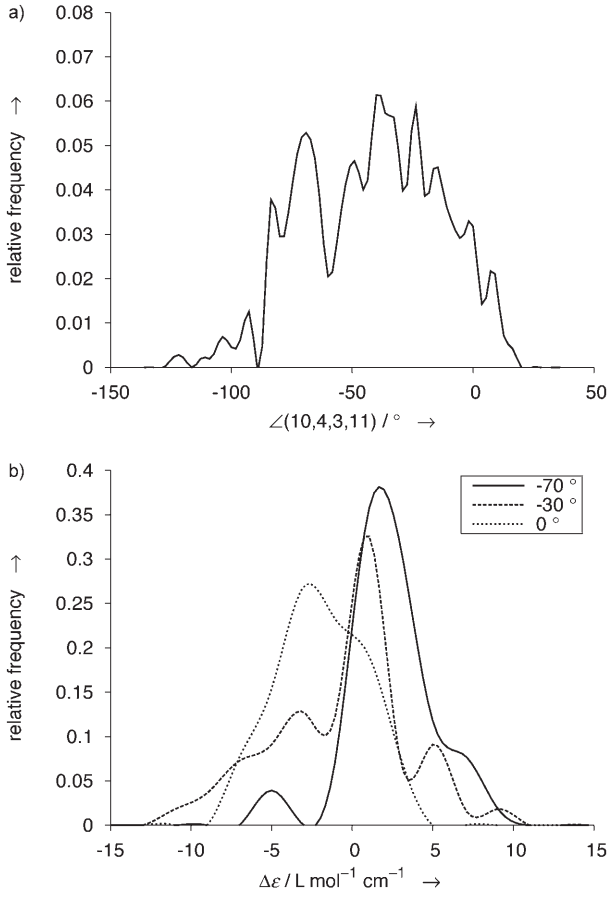

Figure 7. a) Computed distribution of the 10,4,3,11 torsion angle of **4** at 350 K. For the boat conformer, this angle is −16°, while for the chair conformer it is −72°. The histogram width is 4°. b) Computed conditional probability distribution of the CD intensity at 320 nm for various values of the 10,4,3,11 torsion angle at 350 K. The histogram width is $2\,M^{-1}cm^{-1}$. ε is the molar decadic absorption coefficient.

We have performed a similar analysis for the torsion angle $\measuredangle(9,8,1,6)$, which, according to the helicity rule, should determine the sign of the CD band at 220 nm. The results are shown in Figure 8. Note that negative torsion angles are displayed modulo 360° here to obtain smooth curves. The conditional probability distributions for fixed values of $\measuredangle(9,8,1,6)$ in Figure 8b are very broad and exhibit multiple maxima. This implies that the value of $\measuredangle(9,8,1,6)$ alone is not sufficient to determine the CD spectrum at 220 nm for an individual structure. However, there appears to be a correlation to the thermal mean value of the CD, which is shifted to more positive values as $\measuredangle(9,8,1,6)$ increases. Thus, the helicity rule holds only for the thermal average, not for individual geometric structures of **4**.

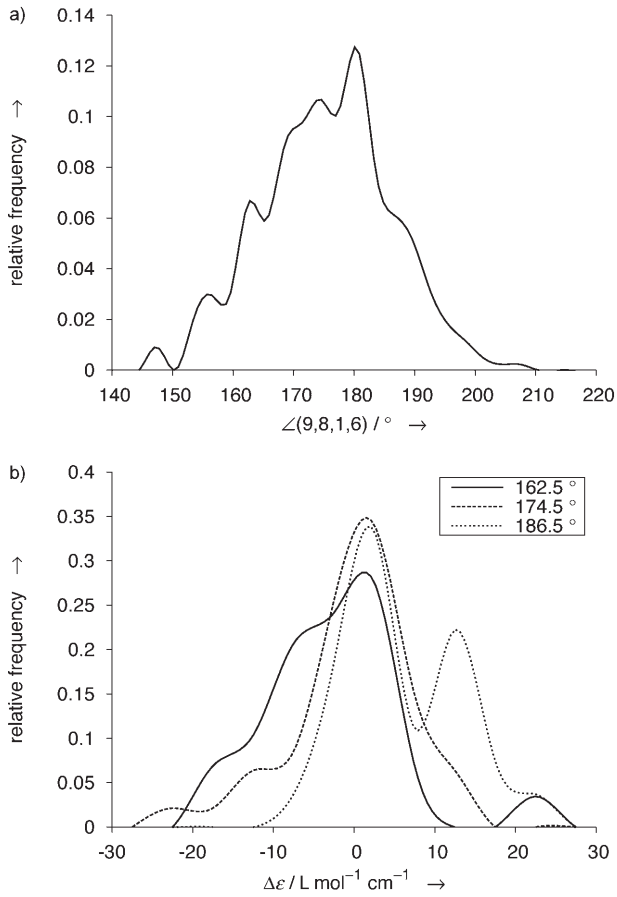

Figure 8. a) Computed distribution of the 9,8,1,6 torsion angle of **4** at 350 K. The histogram width is 3°. b) Computed conditional probability distribution of the CD intensity at 220 nm for various values of the 9,8,1,6 torsion angle at 350 K. The histogram width is $5\,M^{-1}cm^{-1}$. ε is the molar decadic absorption coefficient.

Figure 9 shows the simulated CD spectrum of **4**, as obtained from the MD simulations, in comparison to experiment. The simulated spectrum is in better agreement with the experimental one than the spectra of the individual con-

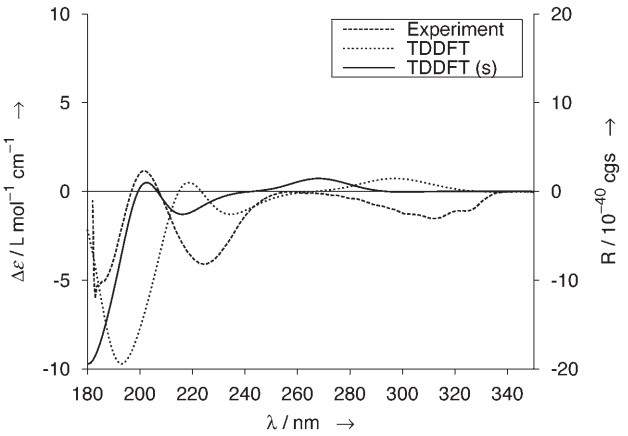

Figure 9. Simulated CD spectrum of **4** at 350 K compared to experiment. The curve denoted (s) was blue-shifted by 0.45 eV. Details as in Figure 1.

formers, although the computed spectrum is red-shifted by 0.45 eV. We expect a red shift compared to the spectrum at 0 K, because thermal motion increases average bond lengths, which generally lowers excitation energies. The sign of the band at 220 nm is correct, as is the shape of the whole spectrum in the 180–250 nm region. The band at 320 nm is less satisfactory; the sign is slightly positive around 300 nm, in contrast to the experimental result. Inspection of the MD data shows that the band at 320 nm results from cancellation of large individual contributions of opposite sign, and its absolute value is only slightly above the statistical uncertainty. In addition, the sign of the 320 nm band depends sensitively on the details of the potential-energy surface. Our present methodology might not be accurate enough to fully account for all these effects.

Carbacepham 5: The lowest energy conformer of carbacepham **5** is predicted to have a chair conformation of the six-membered ring by our calculations (Figure 10), in agreement with simple steric-strain arguments. The only chromophore of **5** that absorbs above 180 nm is the amide group of the azetidin-2-one ring. It is thus surprising that the computed CD spectrum of the lowest energy conformer of **5** has little resemblance to the measured CD spectrum, as is seen in Figure 10: the amide n(O)→π* band is computed with a considerable blue shift; the amide n(N)→π* band at the left end of the spectrum is also blue-shifted and even has the wrong sign.

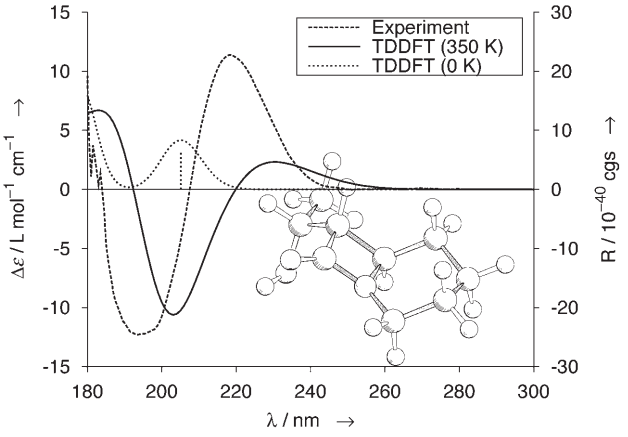

Figure 10. Computed structure of **5** and its simulated CD spectrum at 0 K and 350 K compared to experiment. The 0 K curve corresponds to the conformer shown, while the 350 K curve is the result of MD simulation. Details as in Figure 1.

We performed MD simulations of **5** at 350 K to investigate the impact of thermal effects on the CD spectrum. In contrast to oxacepham **3**, no competing low-energy structure was observed in the simulations. However, the saturated six-membered ring system displayed considerable flexibility. This is illustrated in Figure 11 for the torsion angle ∢(8,1,2,3).

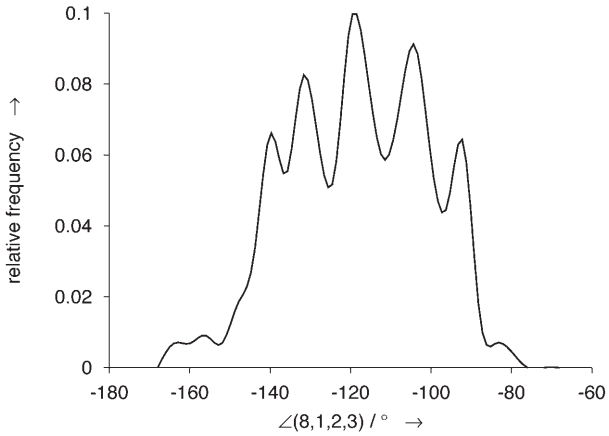

Figure 11. Computed probability distribution of the 8,1,2,3 torsion angle of **5** at 350 K. The histogram width is 4°.

The distribution is broad and unsymmetrical, with a maximum at about −120°, which differs from the value of −115° at 0 K. Again, the CD spectrum was found to depend sensitively on the conformation of both the four- and six-membered rings, with sign inversions occurring for both bands at various points of the MD simulation. The simulated CD spectrum at 350 K compares much better with experiment than that at 0 K (see Figure 10). Both bands are broadened and red-shifted compared to the spectrum at 0 K and have the correct sign.

To provide further evidence for the large thermal effects predicted by the calculations, temperature-dependent measurements of the CD spectrum of **5** were attempted. However, due to the cutoff limits of EPA (diethyl ether/isopentane/ethanol 5/5/2 by vol), a solvent of choice for temperature-dependent CD measurements and solubility issues of **5**, the spectrum of the thioamide of **5** (**5a**, see Experimental Section) had to be used instead of the parent compound. When the temperature was lowered to 253 K, the recorded spectra showed an anomalous intensity decrease for the counterpart of the 220 nm CD band (occurring at 339 nm in the spectrum of **5a**), and a strong suppression of the counterpart of the 200 nm CD band (occurring at 272 nm in the spectrum of **5a**). Both observations support the present calculations,

because one expects an increasing population of the lowest energy conformer at lower temperature, and thus an increasing similarity of the experimental CD spectrum to the computed spectrum at 0 K in Figure 10. The MD simulations suggest that considerably lower temperatures than 253 K are required to fully "freeze out" the lowest energy conformer shown in Figure 10.

Carbacephams 6 and 7: Carbacephams **6** and **7** have phenoxyl substituents at C(7). These phenoxyl groups absorb at similar wavelengths as the amide chromophore, which considerably complicates the CD spectra. The lowest energy conformer of **6** shows a half-chair conformation of the six-membered ring (see Figure 12). Due to the C=C double

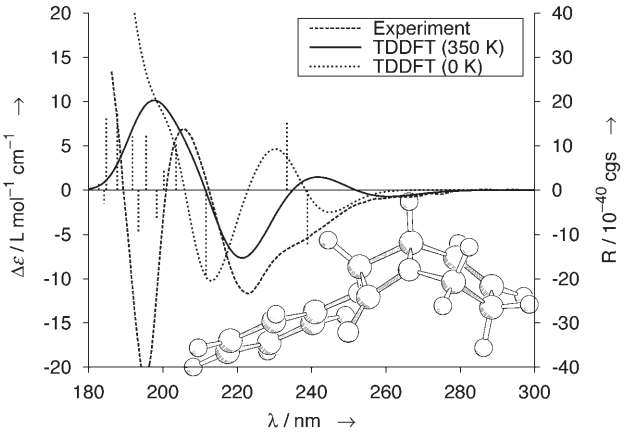

Figure 12. Computed structure of **6** and its simulated CD spectrum at 0 and 350 K compared to experiment. The 0 K curve corresponds to the conformer shown, while the 350 K curve is the result of MD simulation. Details as in Figure 1.

bond between C(4) and C(5), internal rotation of the six-membered ring is restricted. Consistent with our prior observations, this explains why the computed CD spectrum at 0 K differs only slightly from the result of an MD simulation at 350 K (see Figure 12). The shoulder at 240 nm may be assigned to the lowest $\pi \rightarrow \pi^*$ transition of the phenoxyl group, which is split due to interaction with the amide chromophore. The calculations do not capture the peaked negative band present in the experimental spectrum of **6** at about 195 nm. Nevertheless, the agreement between experiment and theory is certainly good enough to confirm the helicity rule once more.

Carbacepham **7** is the most difficult system investigated here, and it demonstrates the limitations of our present theoretical approach. The six-membered ring is conformationally unrestricted, as in **5**, and this suggests large thermal effects on the CD spectrum. However, even the CD spectrum sampled at 350 K does not reproduce the negative band in the experimental spectrum at 220 nm. While we have no definitive explanation for this discrepancy, we observe extreme fluctuations (up to two orders of magnitude of both signs) and intensity bursts in the MD simulations of the 220 nm band; the orientation of the phenoxyl group relative to the amide chromophore seems to play an important role. This implies that the CD spectrum of **7** is especially sensitive to small errors, for example, in the structure, the treatment of solvation effects, or in the electronic coupling between the amide and phenoxyl chromophores, which appears to be unusually large for certain relative orientations. Inverting the configuration of the bridgehead carbon atom produces a CD spectrum very similar to that shown in Figure 13. We conclude that our present methods are not accurate enough to determine the absolute configuration of **7**.

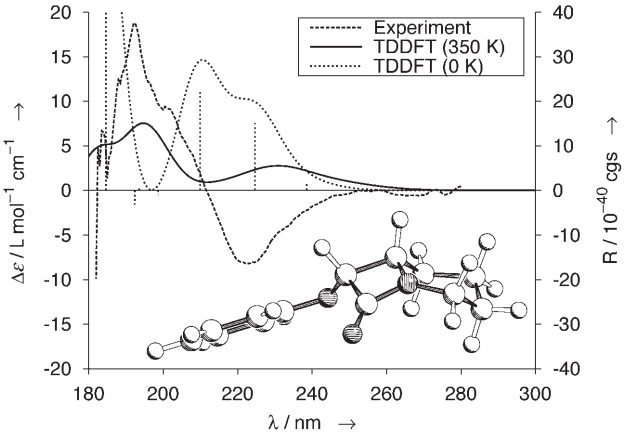

Figure 13. Computed structure of **7** and its simulated CD spectrum at 0 and 350 K compared to experiment. The 0 K curve corresponds to the shown conformer, while the 350 K curve is the result of MD simulation. Details as in Figure 1.

Cepham 8: The six-membered ring of cepham **8** is again in a chair conformation (Figure 14), similar to **1** and **3**. The cyclopropane ring and the large sulfur atom largely restrict the conformational flexibility of the six-membered ring, making MD simulations unnecessary. There are several energetically low-lying conformers of the attached side chains; since their CD spectra do not differ much in the experimentally acces-

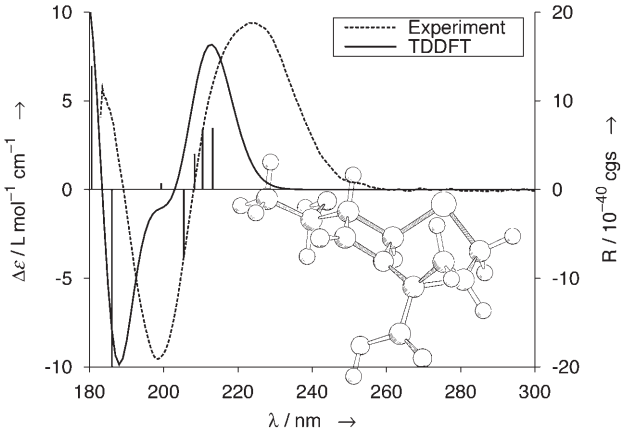

Figure 14. Computed structure of **8** and its simulated CD spectrum compared to experiment. Details as in Figure 1.

sible region, we consider only the energetically most stable structure.

The simulated CD spectrum is in good agreement with experiment. The positive band is due to transitions out of the amide n(N) into the C=O π^* orbital of the adjacent COOH group, the amide n(O)→π^* transition, and transitions out of the sulfur lone pair into the same acceptor orbitals. The negative band at 200 nm mainly results from the carbonyl n→π^* transition of the COOH group, with some admixture of the amide n(O) as donor orbital. With a torsion angle $\measuredangle$(9,8,1,6) of −176°, the helicity rule is satisfied.

Conclusion

The CD spectra of the cepham derivatives studied here depend sensitively on the molecular conformation. Different conformers of the same enantiomer can have radically different CD spectra. The correlation between the three-dimensional molecular structure and individual CD bands is very complex. In particular, the sign and shape of the characteristic 220 nm amide band cannot be predicted from the local conformation of the amide group alone, as was assumed in the derivation of the helicity rule. This is obvious from the failure of the helicity rule for the boat conformers of **2**, **3**, and **4**, where it erroneously predicts the same sign for the 220 nm band as for the chair conformers.

The above applies to the CD spectra of individual conformers at 0 K, to which advanced computational treatments such as TDDFT were limited in the past. However, the experimental CD spectra reported here were measured at room temperature and thus represent a thermal average over the CD spectra of many different conformations. To account for these effects, we performed extensive MD simulations on fully quantum-mechanical Born–Oppenheimer potential-energy surfaces. Except for **7**, where our calculations were inconclusive, we were able to show that the helicity rule holds for all compounds studied in this work if the thermally averaged CD spectra and the thermally averaged torsion and dihedral angles are used.

In view of the elusively complex relation between CD and the structure of individual conformers, this is a surprising result. Scrutiny of the MD trajectories suggests two explanations: 1) The high sensitivity of CD to conformational details even of distant parts of the molecules is considerably reduced in the thermal average; 2) while the energetically lowest conformers of the systems studied here differ considerably in their structure, the regions of configuration space sampled at room temperature are more similar and depend mainly on the absolute configuration of the bridgehead carbon atom. Thus, the helicity rule may yield a good first guess of the absolute configuration of similar compounds at room temperature if the average conformation is close to the average conformation of the cepham derivatives studied here (cf. Table 2). For a more definite assignment of the absolute configuration, however, we strongly recommend confirming the predictions of the helicity rule with high-quality computational results, as was done in the present work. Our calculations of the boat conformers of **2**–**4** suggest that stabilization of the boat form of the six-membered ring, for example, by bulky substituents, might result in a violation of the helicity rule.

The extraordinary sensitivity of CD to the molecular conformation of even distant groups is not entirely surprising from a theoretical point of view, because 1) most molecular excitations are not localized but couple with other chromophores, and 2) even small variations of the molecular structure can entirely change the orientation of transition dipole moments, which strongly affects CD intensities. Nevertheless, an explicit treatment of thermal effect has not been paid much attention in ab initio calculations of molecular CD spectra in the past, possibly because of the high computational cost associated with a proper treatment of these effects. The present work demonstrates that, even for moderately flexible molecules, thermal effects can alter electronic CD spectra qualitatively, and the differences can be comparable to or larger than other sources of error, such as typical shortcomings of present density functionals.

The MD simulations performed here must be distinguished from vibronic model calculations,[26] which were recently applied to the fine structure in the electronic CD spectrum of dimethyloxirane in a TDDFT framework.[22] Vibronic models explicitly account for discrete vibrational level structure, while the present classical treatment of nuclear motion will at best produce a correct spectral envelope. On the other hand, vibronic model calculations are often based on normal-mode expansions and thus cannot easily deal with significant structural changes. Therefore, the domain of such calculations is high-resolution spectroscopy of conformationally restricted molecules. The effects due to conformational dynamics we observe (e.g., in the CD spectrum of **4**) are considerably larger than the vibrational fine structure effects reported in ref. [22a]. At present, we see few alternatives to an MD approach for many larger organic and biomolecular systems exhibiting conformational flexibility.

These conclusions may be interpreted in different ways. On the one hand, our results show that CD simulations for flexible molecules are highly challenging, and emphasize the need for efficient large-scale MD simulations of molecules in solution. Considering the high sensitivity of CD to the molecular conformation we have observed, the suitability of force fields for this purpose should be carefully validated. Depending on the required simulation time, the full DFT Born–Oppenheimer MD simulation employed here is presently suitable for systems with up to about 50 atoms. Propagation methods in the spirit of Car–Parrinello MD reduce the cost of a single time step but require considerably shorter time steps than Born–Oppenheimer MD (cf., however, ref. [27]) and introduce additional approximations. A promising alternative might be to use semi-empirical methods such as tight-binding DFT[28] to generate the trajectories. On the experimental side, low-temperature CD measurements should be pursued to monitor the populations of individual conformers.

On the other hand, with electronic structure calculations enabling us to read and understand the complex information contained in electronic CD spectra, CD spectroscopy may become a powerful tool to investigate details of the molecular structure. The carbonyl group in the oxacephams **3** and **4** exemplifies how spectator chromophores may be used as sensitive "chirality probes" of the molecular conformation. Such chirality probes may eventually be useful for studies of the interaction of β-lactam antibiotics and penicillin-binding proteins or β-lactamases under physiological conditions.

Computational and Experimental Section

Ground-state DFT and TDDFT calculations: Ground-state structures were optimized by using a split-valence basis set with a set of polarization functions at each non-hydrogen atom [SV(P)].[29] SV(P) energetics were validated with larger triple-zeta valence basis sets with two sets of polarization functions at each non-hydrogen atom (def2-TZVP).[30] Fine quadrature grids (size m4[15,31]) were employed. Energies were converged to 1 μhartree and gradients were converged to a maximum norm of 10^{-3} a.u. in the geometry optimizations. All stationary points were confirmed to be minima by force-constant calculations. In the TDDFT calculations, the number of excitations included was chosen to cover the entire range of the experimental spectra (180–400 nm). SV(P) basis sets were used, since exploratory calculations in larger basis sets showed a moderate increase in the CD intensities on diffuse augmentation, and a slight overall shift to longer wavelengths, but no qualitative change. CD spectra were simulated by superposition of Gaussians with a uniform line width of 0.16 eV. Solvent effects were taken into account by the COSMO model[21] using the dielectric constant of acetonitrile (37.5). The fast response of the screening potential was neglected in the TDDFT response calculations. The hybrid density functional of Perdew, Burke, and Ernzerhof (PBE0)[32] was used throughout, unless stated otherwise. Containing 25% of Hartree–Fock exchange, PBE0 is more robust for higher excitation energies[33] and less susceptible to charge-transfer error than other functionals. All calculations were carried out with the TURBOMOLE program suite.[34]

Molecular dynamics simulations: Finite temperature effects on the computed CD spectra were taken into account by fully quantum-mechanical Born–Oppenheimer MD simulations. In these simulations, the ensemble average of an observable A (e.g., a bond angle or the CD intensity) is replaced by its time average by virtue of the ergodic theorem.[35] The time average is computed by propagating the system on the Born–Oppenheimer ground-state potential-energy surface by using a classical description of the nuclei. To this end, we solve the classical equations of motion of the nuclei in finite time steps ("MD steps") τ by means of the Verlet leapfrog algorithm,[36] as available in the FROG module[37] of TURBOMOLE. To simulate the canonical ensemble, the leapfrog algorithm was combined with canonical Nosé–Hoover dynamics[38] for the present work. The thermostat relaxation time was chosen to be four times as large as the time step (see below).

The trajectories were generated as follows: Initial configurations were generated from an 800 K trajectory. Starting from these initial configurations, 22 trajectories were computed at 350 K. Each trajectory comprised 2200 time steps of step length $\tau =$ 25 a.u. (0.6 fs), corresponding to a total simulation time of 29.3 ps. For the sake of efficiency, energies and forces were evaluated with the BP86 functional[39] in combination with the RI-J approximation[31,40] and a small quadrature grid (size 1[15]). Relative conformational energies are rather insensitive to these changes; for example, the energy difference of the chair and boat conformers of **4** changed by about 0.5 kcal mol^{-1}. The ensemble average of A was computed according to Equation (1):

$$\langle A \rangle = \frac{1}{N} \sum_{i=1}^{N} A_i \qquad (1)$$

where N is the number of sampling steps. After an initial equilibration phase of 300 steps, every hundredth step was used to sample structural parameters and CD spectra, corresponding to $N = 440$ in total. The CD spectrum was calculated for each of these 440 configurations as described above.

Source and synthesis of investigated compounds 1–8: The syntheses of compounds **1**–**4**[24] and **8**[25] were described by us before.

Compound **5** was prepared in two steps from already described compound **9**[41] by standard removal of the *tert*-butyldimethylsilyl (TBDMS) group with tetrabutylammonium fluoride (TBAF) followed by catalytic hydrogenation of the double bond on palladium (Scheme 3).

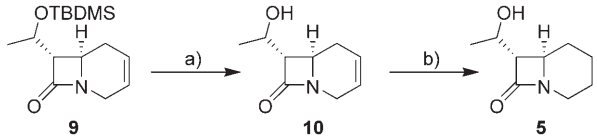

Scheme 3. Synthesis of **5**. a) TBAF, THF, RT, 70%; b) H_2, Pd/C, EtOH, RT, 95%.

Compounds **6** and **7** were prepared by multistep synthesis according to Scheme 4. Known acetonide **11**[42] was treated with *p*-TsOH in boiling THF/water to afford diol **12**. The 1,2-dihydroxy moiety of **12** was then eliminated by reaction with iodine and triphenylphosphine to produce alkene **13**. In the next step the protecting *p*-methoxyphenyl group was removed from the nitrogen atom by treatment of **13** with cerium(IV) ammonium nitrate (CAN) in acetonitrile/water solution at room temperature to yield 3-phenoxy-4-vinyl β-lactam **14**. Lactam **14** was treated with an equivalent amount of sodium hydride and alkylated with 4-bromo-1-butene to afford diene **15**. The diene system in **15** was then subjected to metathesis with nitro-substituted Hoveyda–Grubbs ruthenium catalyst

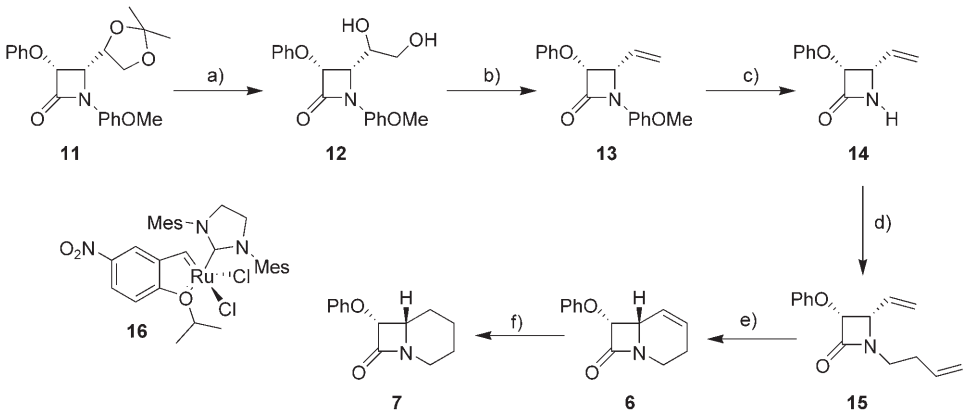

Scheme 4. Synthesis of **6** and **7**. a) *p*-TsOH, THF/H_2O, reflux, 73%; b) Ph_3P, imidazole, I_2, PhMe, reflux, 86%; c) CAN, CH_3CN/H_2O, RT, 50%; d) NaH, 4-bromo-1-butene, DMF, RT, 50%; e) cat. **16**, CH_2Cl_2, 45°C, 80%; f) H_2, Pd/C, EtOH, RT, 95%.

16, recently introduced to synthetic practice,[43] to produce target compound **6**. Target compound **7** was obtained by catalytic hydrogenation of **6** on palladium in ethanol solution at room temperature under standard pressure.

Compound **5a** was prepared from **9** by hydrogenation of a double bond on palladium, replacement of the carbonyl oxygen atom with a sulfur atom by reaction with Lawesson's reagent, and removal of the TBDMS group by reaction with TBAF (Scheme 5).

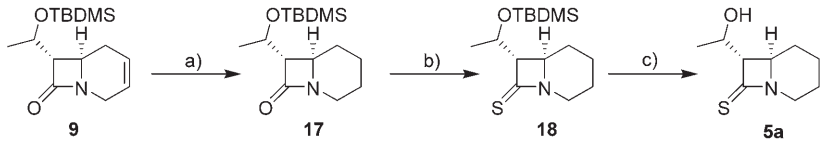

Scheme 5. Synthesis of **5a**. a) H_2, Pd/C, EtOH, RT, 90%; b) Lawesson's reagent, C_6H_6, reflux; c) TBAF, THF, RT, 90%.

General information: IR spectra were recorded with a Perkin Elmer Spectrum 2000. ^{13}C and ^1H NMR spectra were recorded at room temperature in $CDCl_3$ (containing 1% TMS) with a Bruker Avance DRX 500 spectrometer. CD and UV spectra were recorded with a Jasco J-715 spectropolarimeter and a Varian Cary 1E UV/Vis spectrophotometer, respectively. Optical rotation was measured with a Jasco P-1020 polarimeter. Mass spectra and high-resolution mass spectra were obtained with an AMD 604 mass spectrometer. Elemental analyses were performed on an Elementar Vario EL analyzer. Column chromatography was performed on silica gel (Silica Gel 60, 230–400 mesh, Merck). Thin-layer chromatography was performed on Merck TLC aluminium sheets with Silica Gel 60 F_{254}. Solvents were purified according to literature methods before use.[44]

(6*R*,7*S*)-[(1*R*)-1-Hydroxyethyl]-1-azabicyclo[4.2.0]oct-3-en-8-one (10): Tetrabutylammonium fluoride (90 mg, 0.285 mmol) was added to a solution of **9** (40 mg, 0.205 mmol) in THF (4 mL). The mixture was kept at room temperature until the substrate had been consumed (ca. 2 h). Then the solution was diluted with Et_2O (20 mL), washed with water (2× 15 mL), dried with $MgSO_4$, evaporated to dryness, and purified by chromatography on silica gel (5% MeOH in CH_2Cl_2) to produce **10** (16 mg, 67%) as a colorless oil. $[\alpha]_D^{22}=+80.1$ ($c=0.6$, CH_2Cl_2); ^1H NMR (500 MHz, $CDCl_3$): $\delta=5.87$–5.81 (m, 1H), 5.73–6.69 (m, 1H), 4.20 (p, $J=6.3$ Hz, 1H), 4.07 (dq, $J=18.2$, 3.1 Hz, 1H), 3.54 (dp, $J=18.2$, 2.3 Hz, 1H), 3.48 (ddd, $J=9.1$, 5.2, 5.2 Hz, 1H), 2.82 (dd, $J=6.0$, 1.5 Hz, 1H), 2.48 (dtt, $J=16.8$, 5.3, 1.0 Hz, 1H), 2.20–2.12 (m, 1H), 1.33 ppm (d, $J=6.3$ Hz, 3H); ^{13}C NMR (125 MHz, $CDCl_3$): $\delta=167.03$, 123.80, 122.38, 66.44, 65.46, 46.16, 38.31, 28.19, 21.68 ppm; IR (film): $\tilde{\nu}=3403$, 1727 cm^{-1}; HRMS (EI): *m/z*: calcd for $C_9H_{13}NO_2$: 167.09395, found 167.09463.

(6*R*,7*S*)-[(1*R*)-1-Hydroxyethyl]-1-azabicyclo[4.2.0]octan-8-one (5): A mixture of **10** (15 mg, 0.089 mmol), 10% Pd on C (5 mg), and ethanol (3 mL) was placed in a 50 mL round-bottom flask equipped with a magnetic stirring bar, and the flask was attached to an atmospheric hydrogenation apparatus. Then the flask was filled with hydrogen and the components were vigorously stirred until the uptake of hydrogen had been ceased (ca 2.0 mL). Then the mixture was filtered through Celite and the solvent was evaporated to give analytically pure **5** (14 mg, 95%) as a colorless oil. $[\alpha]_D^{22}=+9.6$ ($c=0.5$, CH_2Cl_2); ^1H NMR (500 MHz, $CDCl_3$): $\delta=4.14$ (p, $J=6.1$ Hz, 1H), 3.83 (dd, $J=13.7$, 5.2 Hz, 1H), 3.36 (ddd, $J=10.8$, 4.5, 1.7 Hz, 1H), 2.85 (dd, $J=5.9$, 1.7 Hz, 1H), 2.77–2.70 (m, 1H), 2.16 (br s, 1H), 2.08–2.03 (m, 1H), 1.92–1.85 (m, 1H), 1.67–1.61 (m, 1H), 1.45–1.24 (m, 3H), 1.29 ppm (d, $J=6.3$ Hz, 3H); ^{13}C NMR (125 MHz, $CDCl_3$): $\delta=166.06$, 65.89, 65.34, 50.54, 38.80, 30.34, 24.42, 22.25, 21.57 ppm; IR (film): $\tilde{\nu}=3416$, 1726 cm^{-1}; UV/Vis (acetonitrile): λ_{max} (ε) = 197 nm (7700 $mol^{-1}Lcm^{-1}$); HRMS (EI): *m/z*: calcd for $C_9H_{15}NO_2$: 169.10999, found 169.11028.

(3*R*,4*S*)-4-[(1*R*)-1,2-Dihydroxyethyl]-1-(4-methoxyphenyl)-3-phenoxyazetidin-2-one (12): A mixture of acetonide **11** (800 mg, 2.16 mmol), THF (20 mL), H_2O (7 mL), and *p*-TsOH (138 mg, 1.37 mmol) was refluxed for 24 h. Then the mixture was diluted with aqueous $NaHCO_3$ solution (15 mL) and extracted with AcOEt (3×25 mL). The combined organic layers were dried with $MgSO_4$ and evaporated to dryness. The crude product was crystallized from MeOH to yield **12** (593 mg, 82%) as colorless crystals. M.p. 120–122 °C; $[\alpha]_D^{22}=+116.5$ ($c=1$, $CHCl_3$); ^1H NMR (500 MHz, $CDCl_3$): $\delta=7.49$–7.45 (m, 2H), 7.35–7.33 (m, 2H), 7.15–7.13 (m, 2H), 7.09–7.06 (m, 1H), 6.90–6.86 (m, 2H), 5.39 (d, $J=5.4$ Hz, 1H), 4.59 (t, $J=4.9$ Hz, 1H), 4.31–4.26 (m, 1H), 3.79 (s, 3H), 3.74 ppm (d, $J=5.7$ Hz, 1H); ^{13}C NMR (125 MHz, $CDCl_3$): $\delta=163.55$, 157.27, 157.02, 130.68, 129.82, 123.05, 120.23, 116.02, 114.34, 79.91, 71.54, 63.65, 58.27, 55.50 ppm; IR (film): $\tilde{\nu}=1742$ cm^{-1}; elemental analysis calcd (%) for $C_{18}H_{19}NO_5$: C 65.64, H 5.81, N 4.25; found: C 65.67, H 5.81, N 4.15.

(3*R*,4*S*)-1-(4-Methoxyphenyl)-3-phenoxy-4-vinylazetidin-2-one (13): A solution of iodine (1.0 g, 4.0 mmol) in toluene (50 mL) was added over 0.5 h to a refluxing solution of **12** (875 mg, 2.65 mmol), imidazole (710 mg, 10.4 mmol), and triphenylphosphine (2,7 g; 10.3 mmol) in toluene (50 mL). Refluxing was continued for 5 h and then the mixture was cooled to room temperature. The insoluble material was filtered off. The toluene solution was washed consecutively with aqueous $Na_2S_2O_3$ (30 mL), 1 M NaOH (30 mL), and water (30 mL), dried with $MgSO_4$, and evaporated to dryness. The crude product was purified on silica gel (20–40% AcOEt/hexane) and crystallized from AcOEt/hexane to produce **13** (550 mg, 73%) as colorless crystals. M.p. 101–103 °C; $[\alpha]_D^{22}=+18.7$ ($c=0.5$, CH_2Cl_2); ^1H NMR (500 MHz, $CDCl_3$): $\delta=7.44$–7.40 (m, 2H), 7.31–7.27 (m, 2H), 7.03–6.99 (m, 3H), 6.89–6.85 (m, 2H), 5.98 (ddd, $J=17.3$, 10.3, 8.1 Hz, 1H), 5.56 (d, $J=17.3$ Hz, 1H), 5.44 (d, $J=10.3$ Hz, 1H), 5.41 (d, $J=4.8$ Hz, 1H), 4.83 (dd, $J=8.1$, 4.8 Hz, 1H), 3.79 ppm (s, 3H); ^{13}C NMR (125 MHz, $CDCl_3$): $\delta=162.03$, 157.34, 156.58, 131.57, 130.91, 129.51, 122.53, 122.27, 118.77, 115.60, 114.38, 80.92, 61.18, 55.48 ppm; IR (film): $\tilde{\nu}=1755$ cm^{-1}; elemental analysis calcd (%) for $C_{18}H_{17}NO_3$: C 73.20, H 5.80, N 4.74; found: C 73.13, H 5.87, N 4.80.

(3*R*,4*S*)-3-Phenoxy-4-vinylazetidin-2-one (14): Cerium(IV) ammonium nitrate (3.7 g, 6.8 mmol) was added to a solution of **13** (1.0 g, 3.4 mmol) in acetonitrile (60 mL) and water (30 mL) cooled to 0 °C. The mixture was stirred at room temperature for 1 h. Then the mixture was diluted with AcOEt (100 mL) and washed consecutively with water (3×50 mL), saturated aqueous $NaHCO_3$ (50 mL), and brine (50 mL). The organic layer was dried with $MgSO_4$ and evaporated to dryness. The crude product was purified on silica gel (15–30% AcOEt in hexane) and crystallized from AcOEt/hexane to yield **14** (450 mg, 70%) as colorless crystals. M.p. 136–138 °C; $[\alpha]_D^{22}=-41.3$ ($c=0.5$, CH_2Cl_2); ^1H NMR (500 MHz, $CDCl_3$): $\delta=7.30$–7.26 (m, 2H), 7.01 (tt, $J=7.4$, 1.0 Hz, 1H), 6.99–6.96 (m, 2H), 6.20 (br s, 1H), 5.95 (ddd, $J=17.2$, 10.3, 7.4 Hz, 1H), 5.40 (dt, $J=17.2$, 1.0 Hz, 1H), 5.34 (dd, $J=4.7$, 2.3 Hz, 1H), 5.32 (dt, $J=10.3$, 1.0 Hz, 1H), 4.48 ppm (ddt, $J=7.4$, 4.7, 0.8 Hz, 1H); ^{13}C NMR (125 MHz, $CDCl_3$): $\delta=166.07$, 157.23, 132.88, 129.51, 122.26, 120.49, 115.54, 82.69, 57.31 ppm; IR (film): $\tilde{\nu}=1755$ cm^{-1}; elemental analysis calcd (%) for $C_{11}H_{11}NO_2$: C 69.83, H 5.86, N 7. 40; found: C 69.73, H 5.67, N 7.32.

(3*R*,4*S*)-1-(3-Butenyl)-3-phenoxy-4-vinylazetidin-2-one (15): A solution of **14** (200 mg, 0.946 mmol) in anhydrous DMF (5 mL) was added to a suspension of NaH (46 mg, 1.91 mmol) in anhydrous DMF (2 mL). The mixture was stirred at room temperature under an argon atmosphere until evolution of hydrogen had ceased. Then an excess of 4-bromo-1-butene (625 mg, 4.629 mmol) was dropped into the mixture via syringe and the mixture was stirred at room temperature for 2 h. Then the mixture was diluted with Et_2O (50 mL), washed with water (3×20 mL), dried with $MgSO_4$, evaporated to dryness, and purified by chromatography on silica gel (10–15% AcOEt in hexane) to produce **15** (54 mg, 20%) as a colorless oil. $[\alpha]_D^{22}=-7.6$ ($c=0.5$, CH_2Cl_2); ^1H NMR (500 MHz, $CDCl_3$): $\delta=7.27$–7.24 (m, 2H), 6.99 (tt, $J=7.4$, 1.1 Hz, 1H), 6.96–6.93 (m, 2H), 5.88 (ddd, $J=17.2$, 10.3, 8.8 Hz, 1H), 5.78 (ddt, $J=17.2$, 10.3, 6.7 Hz, 1H), 5.43 (ddd, $J=17.2$, 1.3, 0.7 Hz, 1H), 5.36 (ddd, $J=10.3$, 1.2, 0.4 Hz,

1H), 5.26 (d, $J=4.4$ Hz, 1H), 5.14 (dq, $J=17.2$, 1.6 Hz, 1H), 5.10 (dq, $J=10.3$, 1.6 Hz, 1H), 4.36 (dd, $J=8.8$, 4.4 Hz, 1H), 3.50 (dt, $J=14.0$, 7.3 Hz, 1H), 3.14 (ddd, $J=13.8$, 7.2, 6.5 Hz, 1H), 2.41–2.27 ppm (m, 2H); ^{13}C NMR (125 MHz, $CDCl_3$): $\delta=165.35$, 157.32, 134.70, 131.93, 129.42, 122.33, 122.09, 117.30, 115.53, 81.45, 61.46, 39.63, 31.96 ppm; IR (film): $\tilde{\nu}=1763\ cm^{-1}$; elemental analysis calcd (%) for $C_{15}H_{17}NO_2$: C 74.05, H 7.04, N 5.76; found: C 74.04, H 7.04, N 5.74.

(6*R*,7*S*)-7-Phenoxy-1-azabicyclo[4.2.0]oct-4-en-8-one (6): A mixture of lactam **15** (46 mg, 0.189 mmol), dry dichloromethane (10 mL), and nitro-substituted ruthenium catalyst **16** (2,2 mg, 0.003 mmol) was refluxed under an argon atmosphere for 2 h. Then the solvent was removed and the residue was purified by chromatography on silica gel (10% AcOEt in hexane) to produce **6** (34 mg, 83%) as a colorless oil. $[\alpha]_D^{22}=-223.6$ ($c=0.5$, CH_2Cl_2); ^{1}H NMR (500 MHz, $CDCl_3$): $\delta=7.32$–7.28 (m, 2H), 7.03–6.96 (m, 3H), 6.02–5.96 (m, 1H), 5.76–5.72 (m, 1H), 5.28 (d, $J=4.3$ Hz, 1H), 4.29–4.25 (m, 1H), 4.00 (dd, $J=13.8$, 7.8 Hz, 1H), 2.97 (ddd, $J=13.8$, 10.6, 5.6 Hz, 1H), 2.58–2.48 (m, 1H), 2.11–2.03 ppm (m, 1H); ^{13}C NMR (125 MHz, $CDCl_3$): $\delta=168.32$, 157.48, 129.61, 129.45, 122.33, 122.10, 115.16, 81.12, 51.99, 36.04, 23.39 ppm; IR (film): $\tilde{\nu}=1764\ cm^{-1}$; UV/Vis (acetonitrile): λ_{max} (ε) = 269 (1350), 218 (12000, sh), 194 nm ($37200\ mol^{-1}\,L\,cm^{-1}$); elemental analysis calcd (%) for $C_{13}H_{13}NO_2$: C 72.54, H 6.09, N 6.51; found: C 72.39, H 6.13, N 6.53.

(6*S*,7*R*)-7-Phenoxy-1-azabicyclo[4.2.0]octan-8-one (7): A mixture of **6** (20 mg, 0.093 mmol), 10% Pd on C (5 mg), and ethanol (3 mL) was placed in a 50 mL round-bottom flask equipped with a magnetic stirring bar and the flask was attached to an atmospheric hydrogenation apparatus. Then the flask was filled with hydrogen and the components were vigorously stirred until uptake of hydrogen had been ceased (ca. 2.1 mL). Then the mixture was filtered through Celite and the solvent was evaporated to yield analytically pure **7** (19 mg, 95%) as a colorless oil. $[\alpha]_D^{22}=-93.0$ ($c=0.5$, CH_2Cl_2); ^{1}H NMR (500 MHz, $CDCl_3$): $\delta=7.30$–7.26 (m, 2H), 7.00 (t, $J=7.4$ Hz, 1H), 6.97–6.94 (m, 2H), 5.20 (dd, $J=4.1$, 1.4 Hz, 1H), 3.90 (dd, $J=13.6$, 4.7 Hz, 1H), 3.75 (dt, $J=10.8$, 4.3 Hz, 1H), 2.79–2.72 (m, 1H), 1.93–1.87 (m, 1H), 1.72–1.55 (m, 3H), 1.53–1.38 ppm (m, 2H); ^{13}C NMR (125 MHz, $CDCl_3$): $\delta=164.81$, 157.49, 129.53, 121.93, 115.07, 81.28, 54.12, 38.59, 24.45, 23.82, 21.31 ppm; IR (film): $\tilde{\nu}=1760\ cm^{-1}$; UV/Vis (acetonitrile): λ_{max} (ε) = 269 (1400), 218 (10500, sh), 196 nm ($30500\ mol^{-1}\,L\,cm^{-1}$); elemental analysis calcd (%) for $C_{13}H_{15}NO_2$: C 71.87, H 6.96, N 6.45; found: C 71.60, H 7.21, N 6.46.

(6*R*,7*S*)-7-[(1*R*)-1-(*tert*-butyldimethylsilyl)oxyethyl]-1-azabicyclo-[4.2.0]octan-8-one (17): A mixture of **9** (45 mg, 0.159 mmol), 10% Pd on C (10 mg), and ethanol (7 mL) was placed in a 50 mL round-bottom flask equipped with a magnetic stirring bar and the flask was attached to an atmospheric hydrogenation apparatus. Then the flask was filled with hydrogen and the components were vigorously stirred until uptake of hydrogen had ceased (ca. 3.6 mL). Then the mixture was filtered through Celite and the solvent was evaporated to yield analytically pure **17** (40 mg, 90%) as a colorless oil. $[\alpha]_D^{22}=+2.9$ ($c=0.5$, CH_2Cl_2); ^{1}H NMR (500 MHz, $CDCl_3$): $\delta=4.12$ (p, $J=6.1$ Hz, 1H), 3.81 (dd, $J=13.7$, 4.9 Hz, 1H), 3.31 (ddd, $J=10.8$, 4.4, 1.5 Hz, 1H), 2.76 (dd, $J=5.5$, 1.6 Hz, 1H), 2.71–2.65 (m, 1H), 2.02–1.96 (m, 1H), 1.89–1.84 (m, 2H), 1.44–1.34 (m, 2H), 1.13–1.25 (m, 1H), 1.21 (d, $J=6.2$, 3H), 0.87 (s, 9H), 0.07 (s, 3H), 0.06 ppm (s, 3H); ^{13}C NMR (125 MHz, $CDCl_3$): $\delta=166.12$, 66.40, 65.86, 50.53, 38.55, 30.30, 25.69, 24.44, 22.78, 22.41, 17.91, −4.19, −5.00 ppm; IR (film): $\tilde{\nu}=1752\ cm^{-1}$; HRMS (LSIMS): m/z: calcd for $C_{15}H_{29}NO_2NaSi$ $[M+Na]^+$: 306.18598, found 306.18522.

(6*R*,7*S*)-7-[(1*R*)-1-Hydroxyethyl]-1-azabicyclo[4.2.0]octane-8-thione (5a): A solution of **17** (35 mg, 0.124 mmol) and Lawesson's reagent (25 mg, 0.062 mmol) in benzene (7 mL) was refluxed for 3 h. Then the solvent was removed and the residue filtered through a pad of silica gel (10% AcOEt in hexane). The solvent was removed and the crude product **18** (34 mg, 0.114 mmol) was dissolved in anhydrous THF. TBAF (72 mg, 0.228 mmol) was added to the solution and the reaction mixture was kept at room temperature for 2 h. Then the solution was diluted with Et_2O (20 mL) and washed with water (2×15 mL), dried with $MgSO_4$, evaporated to dryness, and purified by chromatography on silica gel (5% MeOH in CH_2Cl_2) to produce **5a** (23 mg, total yield 81%) as a colorless oil. $[\alpha]_D^{22}=-1.8$ ($c=0.5$, CH_2Cl_2); ^{1}H NMR (500 MHz, $CDCl_3$): $\delta=4.27$–4.19 (m, 2H), 3.90–3.86 (m, 1H), 2.97–2.91 (m, 1H), 2.86 (d, $J=4.4$ Hz, 1H), 2.08–2.02 (m, 2H), 1.95–1.90 (m, 1H), 1.82–1.76 (m, 1H), 1.54–1.40 (m, 3H), 1.30 ppm (d, $J=6.4$ Hz, 3H); ^{13}C NMR (125 MHz, $CDCl_3$): $\delta=198.26$, 66.76, 65.04, 58.70, 41.79, 29.97, 24.16, 21.88, 20.30 ppm; IR (film): $\tilde{\nu}=1442\ cm^{-1}$; HRMS (EI): m/z: calcd for $C_9H_{15}NOS$: 185.08744, found 185.08806.

Acknowledgements

F.F. acknowledges helpful discussions with R. Ahlrichs. The authors are deeply indebted to Dr. K. Grela for providing a sample of nitro-substituted ruthenium catalyst. This work was supported by the Polish State Committee for Scientific Research (KBN), grant No. PBZ-KBN-126/T09/2004, and by the Center for Functional Nanostructures (CFN) of the Deutsche Forschungsgemeinschaft (DFG) within project C3.9.

[1] F. von Nussbaum, M. Brands, K. Hinzen, S. Weigand, D. Häbich, *Angew. Chem.* **2006**, *118*, 5194–5254; *Angew. Chem. Int. Ed.* **2006**, *45*, 5072–5129.

[2] J. F. Fisher, S. O. Meroueh, S. Mobashery, *Chem. Rev.* **2005**, *105*, 395–424.

[3] R. B. Morin, M. E. Gorman, *Chemistry and Biology of β-Lactam Antibiotics*, Academic Press, New York, **1982**.

[4] a) A. G. Brown, D. Butterworth, M. Cole, G. Hanscomb, J. D. Hood, C. Reading, G. N. Rolinson, *J. Antibiot.* **1976**, *29*, 668–669; b) A. G. Brown, D. F. Corbett, J. Goodacre, J. B. Harbridge, T. T. Howarth, R. J. Ponsford, I. Stirling, T. I. King, *J. Chem. Soc. Perkin Trans. 1* **1984**, 635–650.

[5] L. D. Cama, B. G. Christensen, *J. Am. Chem. Soc.* **1974**, *96*, 7582–7584.

[6] R. A. Firestone, J. L. Fahey, N. S. Maciejewicz, G. S. Patel, B. G. Christensen, *J. Med. Chem.* **1977**, *20*, 551–556.

[7] a) D. B. Brown, R. J. Evans, *J. Chem. Soc. Chem. Commun.* **1979**, 282–283; b) H. U. Naegeli, H. R. Loosli, A. Nussbaumer, *J. Antibiot.* **1986**, *39*, 516–524.

[8] B. Alcaide, P. Almendros, *Curr. Med. Chem.* **2004**, *11*, 1921–1949.

[9] a) H. Ogura, H. Takayanagi, K. Kubo, K. Furuhata, *J. Am. Chem. Soc.* **1973**, *95*, 8056–8059; b) D. B. Boyd, J. P. Riehl, F. S. Richardson, *Tetrahedron* **1979**, *35*, 1499–1508.

[10] R. Łysek, K. Borsuk, M. Chmielewski, Z. Kałuża, Z. Urbańczyk-Lipkowska, A. Klimek, J. Frelek, *J.Org.Chem.* **2002**, *67*, 1472–1479.

[11] T. T. Danh, W. Bocian, L. Kozerski, P. Szczukiewicz, J. Frelek, M. Chmielewski, *Eur. J. Org. Chem.* **2005**, 429–440.

[12] J. Frelek, R. Łysek, K. Borsuk, J. Jagodziński, B. Furman, A. Klimek, M. Chmielewski, *Enantiomer* **2002**, *7*, 107–114.

[13] a) F. Furche, R. Ahlrichs, C. Wachmann, E. Weber, A. Sobanski, F. Vögtle, S. Grimme, *J. Am. Chem. Soc.* **2000**, *122*, 1717–1724; b) J. Autschbach, S. Patchkovskii, T. Ziegler, S. J. A. Van Gisbergen, E. J. Baerends, *J. Chem. Phys.* **2002**, *117*, 581–592; c) C. Diedrich, S. Grimme, *J. Phys. Chem. A* **2003**, *107*, 2524–2539; d) M. Pecul, K. Ruud, T. Helgaker, *Chem. Phys. Lett.* **2004**, *388*, 110–119; e) D. Rappoport, F. Furche in *Time-Dependent Density Functional Theory* (Eds.: M. Marques, C. A. Ullrich, F. Nogueira, A. Rubio, K. Burke, E. K. U. Gross), Springer, Berlin, **2006**, pp. 337–354.

[14] M. Pecul, K. Ruud, A. Rizzo, T. Helgaker, *J. Chem. Phys.* **2004**, *108*, 4269–4272.

[15] O. Treutler, R. Ahlrichs, *J. Chem. Phys.* **1995**, *102*, 346–354.

[16] F. Furche, J. P. Perdew, *J. Chem. Phys.* **2006**, *124*, 044103.

[17] F. Furche, D. Rappoport in *Computational Photochemistry, Theoretical and Computational Chemistry, Vol. 16* (Ed.: M. Olivucci), Elsevier, Amsterdam, **2005**, pp. 93–128.

[18] a) I. Demachy, J. Ridard, H. Laguitton-Pasquier, E. Durnerin, G. Vallverdu, P. Archirel, B. Levy, *J. Phys. Chem. B* **2005**, *109*, 24121–24133; b) G. Bringmann, J. Mühlbacher, C. Repges, J. Fleischhauer, *J. Comput. Chem.* **2001**, *22*, 1273–1278; c) D. Seebach, J. V. Schreib-

er, S. Ablele, X. Daura, W. F. van Gunsteren, *Helv. Chim. Acta* **2000**, *83*, 34–57.
[19] L. Bernasconi, J. Blumberger, M. Sprik, R. Vuilleumier, *J. Chem. Phys.* **2004**, *121*, 11885–11899.
[20] R. Car, M. Parrinello, *Phys. Rev. Lett.* **1985**, *55*, 2471–2474.
[21] A. Klamt, G. Schürmann, *J. Chem. Soc. Perkin Trans. 2* **1993**, *5*, 799–805.
[22] a) J. Neugebauer, E. J. Baerends, M. Nooijen, J. Autschbach, *J. Chem. Phys.* **2005**, *122*, 234305; b) M. Nooijen, *Int. J. Quantum Chem.* **2006**, *106*, 2489–2510.
[23] B. C. Mort, J. Autschbach, *J. Phys. Chem. A* **2006**, *110*, 11381–11383.
[24] Z. Kałuża, A. Kazimierski, K. Lewandowski, K. Suwińska, B. Szczêsna, M. Chmielewski, *Tetrahedron* **2003**, *59*, 5893–5903.
[25] A. Korda, J. Winiarski, *Biorgan. Med. Chem.* **2003**, *11*, 1957–1967.
[26] H. Köppel, W. Domcke, L. S. Cederbaum, *Adv. Chem. Phys.* **1984**, *57*, 59–246.
[27] T. D. Kühne, M. Krack, F. R. Mohammed, M. Parrinello, *Phys. Rev. Lett.* **2007**, *98*, 066401.
[28] M. Elstner, D. Porezag, G. Jungnickel, J. Elsner, M. Haugk, T. Frauenheim, S. Suhai, G. Seifert, *Phys. Rev. B* **1998**, *58*, 7260–7268.
[29] A. Schäfer, H. Horn, R. Ahlrichs, *J. Chem. Phys.* **1992**, *97*, 2571–2577.
[30] F. Weigend, R. Ahlrichs, *Phys. Chem. Chem. Phys.* **2005**, *7*, 3297–3305.
[31] K. Eichkorn, F. Weigend, O. Treutler, R. Ahlrichs, *Theor. Chem. Acc.* **1997**, *97*, 119–124.
[32] J. P. Perdew, M. Ernzerhof, K. Burke, *J. Chem. Phys.* **1996**, *105*, 9982–9985.
[33] C. Adamo, G. E. Scuseria, V. Barone, *J. Chem. Phys.* **1999**, *111*, 2889–2899.
[34] a) R. Ahlrichs, M. Bär, M. Häser, H. Horn, C. Kölmel, *Chem. Phys. Lett.* **1989**, *162*, 165–169; b) http://www.turbomole.com.
[35] M. P. Allen, D. J. Tildesley, *Computer Simulation of Liquids*, Oxford University Press, Oxford, **1987**.
[36] L. Verlet, *Phys. Rev.* **1967**, *159*, 98–103.
[37] S. D. Elliott, R. Ahlrichs, O. Hampe, M. M. Kappes, *Phys. Chem. Chem. Phys.* **2000**, *2*, 3415–3424.
[38] W. G. Hoover, *Phys. Rev. A* **1985**, *31*, 1695–1697.
[39] a) A. D. Becke, *Phys. Rev. A* **1988**, *38*, 3098–3100; b) J. P. Perdew, *Phys. Rev. B* **1986**, *33*, 8822–8824.
[40] K. Eichkorn, O. Treutler, H. Öhm, M. Häser, R. Ahlrichs, *Chem. Phys. Lett.* **1995**, *242*, 652–660.
[41] A. G. M. Barett, S. P. D. Baugh, D. C. Braddock, K. Flack, V. C. Gibson, M. R. Giles, E. L. Marshall, P. A. Procopiou, A. J. P. White, D. J. Williams, *J. Org. Chem.* **1998**, *63*, 7893–7907.
[42] D. R. Wagle, C. Garai, J. Chiang, M. G. Monteleone, B. E. Kurys, T. W. Strohmeyer, V. R. Hegde, M. S. Manhas, A. K. Bose, *J. Org. Chem.* **1988**, *53*, 4227–4236.
[43] A. Michrowska, R. Bujok, S. Harutyunyan, V. Sashuk, G. Dolgonos, K. Grela, *J. Am. Chem. Soc.* **2004**, *126*, 9318–9325.
[44] D. D. Perrin, W. L. F. Armarego, D. R. Perrin, *Purification of Laboratory Chemicals*, Pergamon Press, Oxford, **1980**.

Received: January 24, 2007
Published online: May 16, 2007

